

Network-Aware Optimization of Distributed Learning for Fog Computing

Yuwei Tu, Yichen Ruan, Su Wang, Satyavrat Wagle,
Christopher G. Brinton, *Senior Member, IEEE*, and Carlee Joe-Wong, *Member, IEEE*

Abstract—Fog computing promises to enable machine learning tasks to scale to large amounts of data by distributing processing across connected devices. Two key challenges to achieving this goal are (i) heterogeneity in devices’ compute resources and (ii) topology constraints on which devices can communicate with each other. We address these challenges by developing the first network-aware distributed learning optimization methodology where devices optimally share local data processing and send their learnt parameters to a server for aggregation at certain time intervals. Unlike traditional federated learning frameworks, our method enables devices to offload their data processing tasks to each other, with these decisions determined through a convex data transfer optimization problem that trades off costs associated with devices processing, offloading, and discarding data points. We analytically characterize the optimal data transfer solution for different fog network topologies, showing for example that the value of offloading is approximately linear in the range of computing costs in the network. Our subsequent experiments on testbed datasets we collect confirm that our algorithms are able to improve network resource utilization substantially without sacrificing the accuracy of the learned model. In these experiments, we also study the effect of network dynamics, quantifying the impact of nodes entering/exiting the network on model learning and resource costs.

Index Terms—federated learning, offloading, fog computing

I. INTRODUCTION

New technologies like autonomous cars and smart factories are coming to rely extensively on data-driven machine learning (ML) algorithms [2]–[4] to produce near real-time insights based on historical data. Training ML models at realistic scales, however, is challenging, given the enormous computing power required to process today’s data volumes. The collected data is also dispersed across networks of devices, while ML models are traditionally managed in a centralized manner [5].

Fortunately, the rise in data generation in networks has been accompanied by a corresponding rise in the computing power of networked devices. Thus, a possible solution for training and making real-time inferences from data-driven ML algorithms lies in the emerging paradigm of fog computing, which aims to design systems, architectures, and algorithms that leverage an aggregation of device capacities between the network edge and cloud [6]. Deployment of 5G wireless networks and the Internet of Things (IoT) is accelerating

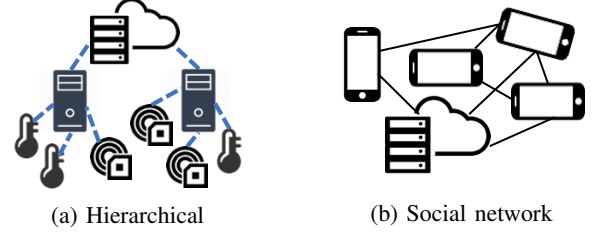


Fig. 1: Cartoon illustrations of two example topologies for fog computing that we consider. In the hierarchical case, less powerful devices are connected to more powerful ones, while for the social network, connections are denser and devices tend to be similar.

adoption of this computing paradigm by expanding the set of connected devices with compute capabilities and enabling direct device-to-device communications [7]. Though centralized ML algorithms are not optimized for such environments, distributed data analytics is expected to be a major driver of 5G adoption [8].

Initial efforts in decentralizing ML have focused on decomposing model parameter updates over several nodes, typically managed by a centralized serving entity [9], [10]. Most of these methods, however, implicitly assume idealized network topologies where node and link properties are homogeneous. Fog environments, by contrast, are characterized by devices’ heterogeneity both in available compute resources and in connectivity with each other, e.g., due to power constraints, mobility, or privacy considerations. For example, consider the two common fog topologies depicted in Figure 1. In the hierarchical scenario, less powerful edge devices are connected to more powerful nodes like edge servers. In the social network case, devices tend to have similar compute resources, but connectivity may vary significantly depending on levels of trust between users [11].

A central question that arises, then, in adapting ML methodologies to fog environments is: *How should each fog device contribute to the ML training and inference?* We answer this question by developing a methodology for *optimizing the distribution of processing across a network of fog devices*.

A. Machine Learning in Fog Environments

ML models are generally trained by iteratively updating estimates of parameter values, such as weights in a neural network, that best “fit” empirical data through data processing at a node or set of devices. We face two major challenges in adapting such training to fog networking environments: (i) *heterogeneity in devices’ compute resources* and (ii) *constraints*

This work was presented in part at the 2020 IEEE Conference on Computer Communications (INFOCOM) [1].

S. Wang and C. Brinton are with the School of Electrical and Computer Engineering at Purdue University. email: {wang2506,cgb}@purdue.edu

Y. Ruan, S. Wagle, and C. Joe-Wong are with the Department of Electrical and Computer Engineering at Carnegie Mellon University. email: {yichenr, srwagle, cjowong}@andrew.cmu.edu

on devices' abilities to communicate with each other. We outline these characteristics, and the potential benefits enabled by our network-aware distributed learning methodology, in some key applications below:

Privacy-sensitive applications. Many ML applications learn models on sensitive user data, e.g., for health monitoring [4]. Due to privacy concerns, most of these applications have devices train their models on local data to avoid revealing data to untrustworthy nodes [11]. Offloading ML data processing to trusted devices, e.g., those owned by friends, however, can reduce training times and improve model accuracy.

Internet-connected vehicles can collaboratively learn about their environment [2], e.g., by combining their data with that of road sensors to infer current road or traffic conditions. Since sensors have less computing capabilities than vehicles, they will likely offload their data to vehicles or roadside units for processing. This offloading must adapt as vehicles move and their connectivity with (stationary) sensors changes.

Augmented reality (AR) uses ML algorithms for e.g., image recognition [3] to overlay digital content onto users' views of an environment. A network of AR-enabled devices can distributedly train ML models, but may exhibit significant heterogeneity: they can range from generic smartphones to AR-specific headsets, with different battery levels. As the users move, connectivity between devices will also change.

Industrial IoT. 5G networks will allow sensors that power control loops in factory production lines to communicate across the factory floor [2], [12], enabling distributed ML algorithms to use this data for, e.g., predicting production delays. It is an open question to determine which controllers should process data from which sensors: this depends on sensor-controller connectivities, which may vary with factory activity.

B. Outline and Summary of Contributions

First, Section II differentiates our work from relevant literature. To the best of our knowledge, we are the first to optimize the distribution of ML data processing (i.e., training) tasks across fog nodes, leading to several contributions:

Formulating the task distribution problem (Section III). In deciding which devices should process which datapoints, our formulation accounts for resource limitations and model accuracy. While ideally more of the data would be processed at devices with more computing resources, sending data samples to such devices may overburden the network. Moreover, processing too many data samples can incur large processing costs relative to the gain in model accuracy. We derive new bounds (Theorem 1) on the model accuracy when data can be moved between devices, and show that the optimal task distribution problem can be formulated as a convex optimization that can be solved rapidly even for large networks.

Characterizing the optimal task distribution (Section IV). Solving the optimization problem formulated in Section III requires specifying network characteristics that may not be known in advance, e.g., the number of datapoints that each device can process in a single timeslot. We analyze the expected deviations from our assumptions in Section III to

derive guidelines on how these characteristics should be set (Theorem 2). We then derive the optimal task distributions for typical fog network topologies (Theorems 3 and 4) and use them to estimate the value (i.e., reduction in processing costs) of allowing devices to move processing tasks to other devices (Theorems 5 and 6).

Experimental validation (Section V). We train classification models on the MNIST dataset to validate our algorithms. We use data traces from a Raspberry Pi testbed to emulate network delays and compute resource availability. Our proposed algorithm nearly halves the processing overhead yet achieves an accuracy comparable to centralized model training.

We discuss potential extensions of our work and conclude in Section VI.

II. RELATED WORK

We contextualize our work within prior results on (i) federated learning algorithms and (ii) methods for offloading ML tasks from mobile devices to edge servers.

A. Federated Learning

In classical distributed learning, multiple “workers” each compute a gradient or parameter value on their own local data. These results are aggregated at a central server, and updated parameter values are sent back to the workers to begin another round of local computations. In the federated learning framework, devices instead perform a *series* of local updates between aggregations [10], [13], [14]. Such a framework preserves user privacy by keeping data at local devices [15] and reduces the communication between devices and the central server.

Since its proposition in [10], federated learning has generated significant research interest; see [16] for a comprehensive survey. Compared to traditional distributed learning, federated learning introduces two new challenges: firstly, data may not be identically or independently distributed as devices locally generate them; and secondly, devices may have limited ability to perform gradient descent due to resource constraints. Many works have attempted to address the first challenge, for instance [17] shares small subsets of user data while achieving significant gains in model accuracy and [18] trains user-specific models under a multi-task learning framework to fit these user-specific models together. When the devices attempt to learn a single model, recent efforts have considered optimizing the frequency of parameter aggregations according to available network and computing resources [5], or adopting a peer-to-peer framework in which parameter updates are shared with neighboring devices instead of a central server [19].

Existing research has also sought to minimize the communication costs in federated scenarios. [20] proposes two methods to reduce uplink communication costs: restricting the parameter space in structured updates or compressing results in sketched updates. Other works attempt to transmit only sparse sets of gradient update results. [21] proposes thresholding updates such that only important gradient updates are transmitted while [22] only communicates the most important individual gradient results, [23] broadens the results in [22] such that

both downlink and uplink communications are compressed, [24] aggregates subsets of the network, and [25] utilizes aggregations between one-hop neighbors instead of the entirety of the network. In regards to optimizing the training process in federated settings, [26] optimizes the training time and power consumption in a federated wireless system. However, to the best of our knowledge, these works neither optimally distribute parameter computations between devices nor simultaneously optimize the compute-communication tradeoffs inherent in fog scenarios. We do both in our prior work [1] and this extension.

B. Offloading

The new paradigm of fog computing introduces computational-optimization opportunities through pooling resources and maximizing idle computational/storage power [6]. Offloading mechanisms take advantage of available devices with computing capabilities to optimize resource-intensive activities. Applied to machine learning tasks, offloading can improve system performance when there are high-bandwidth connections available to alleviate the load on constrained mobile devices, low-power sensors, and embedded medical devices, for example. Use of offloading significantly accelerated the training of a linear regression model in [27] and inference on a neural network in [28]. Existing literature has also considered splitting deep neural networks at the layer level to improve convergence speed. [29] sped up inference by solving a min-cut problem and proposed two network-dependent schemes to accelerate the training phase while [30] developed an architecture wherein edge devices would rely on local inferences when reliable and transmit uncertain classification results to the cloud, to take advantage of the cloud's more complex neural network.

Literature relevant to offloading in fog computing environments tends to emphasize maximizing total computations or minimizing total cost. For instance, in [31], Xu et al. focus on deep learning at the edge in 5G networks and minimize the total time taken by deep learning tasks via offloading computations to different computing infrastructures. Similarly, [32] addresses a scheduling problem in order to maximize the total tasks completed in an edge environment. A recent survey [33] of research on deep learning in edge computing indicates that most works formulate optimization problems based on minimizing total communication cost without factoring in model loss. We instead consider generic ML frameworks, develop an optimization problem to minimize cost while maximizing model accuracy, and use this formulation to provide theoretical performance bounds not found in these prior works.

III. MODEL AND OPTIMIZATION FORMULATION

In this section, we define models for fog networks (Section III-A) and ML training (Section III-B), and then formulate the ML task distribution optimization problem (Section III-C).

A. Fog Computing System Model

Fog computing nodes. We consider a set V of n devices, an aggregation server s , and discrete time intervals $t = 1, \dots, T$.

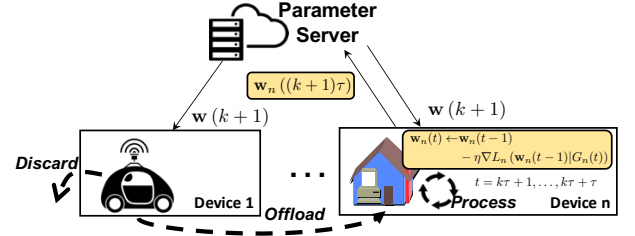


Fig. 2: Federated learning updates between aggregations k and $k+1$. Device 1 discards all of its data or offloads it to device n , which computes τ gradient updates on its local data. The final parameter values are averaged at the parameter server, with the result sent back to the devices to begin a new iteration.

Each device, e.g., a sensor or smartphone, can both collect data and process it to contribute to an ML task. The server s aggregates the results of each device's local analysis, as will be explained in Section III-B. Both the length and number of time intervals may depend on the specific ML application. In each interval t , we suppose a subset of devices $V(t)$, indexed by i , is active (i.e., available to collect and/or process data). For simplicity of notation, we omit i 's dependence on t .

Data collection and processing. We use $D_i(t)$ to denote the set of data collected by device $i \in V(t)$ at time t ; $d \in D_i(t)$ denotes each datapoint. Note, $D_i(t) = \{\}$ if a device does not collect data. $G_i(t)$, by contrast, denotes the set of datapoints *processed* by each device at time t ; our optimization problem in Section III-C relates $G_i(t)$ to the datasets $D_i(t)$. In conventional learning frameworks, $D_i(t) = G_i(t)$, as all devices process the data they collect [5]; separating these variables is one of our main contributions. We suppose that each device i can process up to $C_i(t)$ datapoints at each time t , where $c_i(t)$ represents the average cost per datapoint of processing $C_i(t)$ datapoints at device i and at time t . These might, for example, represent the battery level; devices with low battery will have lower capacities $C_i(t)$ and higher costs $c_i(t)$.

Fog network connectivity. The devices V are connected to each other via a set E of directed links, with $(i, j) \in E$ denoting a link from device i to j , and $E(t) \subseteq E$ denoting the set of functioning links at time t . The overall system then can be described as a directed graph $(\{s, V\}, E)$ with vertices V representing the devices and edges E the links between them. We suppose that $(\{s, V(t)\}, E(t))$ is fully connected at each time t and that links between devices are single-hop, i.e., devices do not use each other as relays except possibly to the server. Note that the scenarios outlined in Section I-A each possess such an architecture: in smart factories, for example, a subset of the floor sensors connect to each controller. Each link $(i, j) \in E(t)$ is characterized by a capacity $C_{ij}(t)$, determined by the bandwidth of the link between devices i and j , i.e. the maximum datapoints it can transfer, and a “cost of connectivity” $c_{ij}(t)$. This cost may reflect network conditions (e.g., signal strengths, congestion) or a desire for privacy, and will be high if sending from i to j is less desirable at t .

Data structure. Each datapoint d can be represented as (x_d, y_d) , where x_d is an attribute/feature vector and y_d is an associated label for model learning. We use $D_V = \cup_{i,t} D_i(t)$ to denote the full set of datapoints collected by all devices over all time. For simplicity, we follow prior work [34], [35] and

model the data collection at device i as points being selected uniformly at random from a (usually unknown) distribution \mathcal{D}_i . In practice the \mathcal{D}_i can evolve over time, but we assume this evolution is slow compared to the horizon T . We use $\mathcal{D} = \cup_i \mathcal{D}_i$ to denote the global distribution induced by these \mathcal{D}_i . Note this assumption implies the relationship between x_d and y_d is temporally invariant, which is common in ML applications, e.g., image recognition from cameras at fixed locations or AR users with random mobility patterns. We will use such an image dataset for evaluation in Section V.

B. Machine Learning Model

Our goal is to learn a parameterized model that outputs y_d given the input feature vector x_d . We use the vector w to denote the set of model parameters, whose values are chosen so as to minimize a loss function $L(w|\mathcal{D})$ that depends on the ML model (e.g., squared error for linear regression, cross-entropy loss for multi-class classifiers [36]). Since the overall distributions \mathcal{D}_i are unknown, instead of minimizing $L(w|\mathcal{D})$ we minimize the empirical loss function, as commonly done:

$$\underset{w}{\text{minimize}} \quad L(w|D_V) = \frac{\sum_{t=1}^T \sum_{i \in V(t)} \sum_{d \in G_i(t)} l(w, x_d, y_d)}{|D_V|} \quad (1)$$

where $l(w, x_d, y_d)$ is the error for datapoint d , and $|D_V|$ is the number of datapoints. Note that the function l may include regularization terms that aim to prevent model overfitting [10].

Fog computing allows (1) to be solved distributedly: instead of computing the solution at the server s , we can use computations at each device i . Below, we follow the commonly used federated averaging framework [5] in specifying these local computations and global aggregation, illustrated by device n in Figure 2. To avoid excessive re-optimization at each device, we suppose that they execute the same local updating algorithm regardless of $G_i(t)$. We adjust the server averaging to account for the amount of data each device processes.

1) *Local loss minimization*: In order to solve (1) in a distributed manner, we first decompose the empirical loss function into a weighted sum of local loss functions

$$L_i(w_i|G_i) = \frac{\sum_{t=1}^T \sum_{d \in G_i(t)} l(w, x_d, y_d)}{|G_i|} \quad (2)$$

where $G_i \equiv \cup_{t \leq T} G_i(t)$ denotes the set of datapoints processed by device i over all times. The global loss in (1) is then equal to $L(w|D_V) = \sum_i L_i(w|G_i) |G_i| / |D_V|$ if $\cup_i G_i = D_V$, i.e., if all datapoints $d \in D_V$ are eventually processed at some device.

Due to the inherent complexity of most ML models, loss functions such as (2) are typically minimized using gradient descent techniques [10]. Specifically, the devices update their local parameter estimates at t according to

$$w_i(t) = w_i(t-1) - \eta(t) \nabla L_i(w_i(t-1)|G_i(t)) \quad (3)$$

where $\eta(t) > 0$ is the step size, which often decreases with t , and $\nabla L_i(w_i(t-1)|G_i(t)) = \sum_{d \in G_i(t)} \nabla l(w_i(t-1), x_d, y_d) / |G_i(t)|$ is the gradient with respect to w of the average loss of points in the current dataset $G_i(t)$ at the

parameter value $w_i(t-1)$. We define the loss only on the current dataset $G_i(t)$ since future data in G_i has not yet been revealed; since we assume each node's data is i.i.d. over time, we can view $L_i(w_i(t-1)|G_i(t))$ as approximating the local loss $L_i(w_i|G_i)$. One can then interpret the computational cost $c_i(t)$ of processing datapoint d as the cost of computing the gradient $\nabla l(w_i(t-1), x_d, y_d)$. If the local data distributions \mathcal{D}_i are all the same, then all datapoints across devices are i.i.d. samples of this distribution, and this process is similar to stochastic gradient descent with batch size $|G_i(t)|$.

2) *Aggregation and synchronization*: The aggregation server s will periodically average the local estimates $w_i(t)$ from the devices and synchronize the devices with a global update. Formally, the k th aggregation is computed as

$$w(k) = \frac{\sum_i H_i(k\tau) \cdot w_i(k\tau)}{\sum_i H_i(k\tau)} \quad (4)$$

where τ is the fixed aggregation period and $H_i(k\tau) = \sum_{t=(k-1)\tau+1}^{k\tau} |G_i(t)|$ is the number of datapoints node i processed since the last aggregation. Thus, the update is a weighted average factoring in the sample size H_i on which each $w_i(t)$ is based. Once this is computed, each device's local estimate is synchronized, i.e., $w_i(t) \leftarrow w(t/\tau)$. A lower value of τ will result in faster convergence of w , while a higher value requires less network resources. Prior work [5] has considered how to optimize τ , so we assume it is pre-determined in our formulation, analyzing its effect experimentally in Section V.

C. Optimization Model for Data Processing Tasks

We now consider the choice of $G_i(t)$, which implicitly defines the ML tasks to be executed by device i at time t , i.e., processing all datapoints in $G_i(t)$. There are two possible reasons $G_i(t) \neq D_i(t)$: first, device i may *offload* some of its collected data to another device j or vice versa, e.g., if i does not have enough capacity ($D_i(t) \geq C_i(t)$) or possibly if j has lower computing costs ($c_j(t) \leq c_i(t)$). Second, device i may *discard* data if processing it does not reduce the empirical loss (1) by much. In Figure 2, device 1 offloads or discards all of its data. We collectively refer to discarding and offloading as *data movement*. We do not include the cost of communicating parameter updates to/from the server in our model; unless a device processes no data, the number of updates stays constant.

1) *Data movement model*: We define $s_{ij}(t) \in [0, 1]$ as the fraction of data collected at device i that is offloaded to device $j \neq i$ at time t . Thus, at time t , device i offloads $D_i(t)s_{ij}(t)$ amount of data to j .¹ Similarly, $s_{ii}(t)$ will denote the fraction of data collected at time t that device i also processes at time t . We suppose that as long as $D_i(t)s_{ij}(t) \leq C_{ij}(t)$, the capacity of the link between i and $j \neq i$, then all offloaded data will reach j within one time interval and be processed at device j in time interval $t+1$. Since devices must have a link between them to offload data, $s_{ij}(t) = 0$ if $(i, j) \notin E(t)$. We also define $r_i(t) \in [0, 1]$ as the fraction of data collected by device i at time t that will be discarded. In doing so, we assume that device j will not discard data that has been offloaded to it

¹For notational convenience, $D_i(t)$ here refers to the length $|D_i(t)|$, and similarly for $G_i(t)$ in this section. The context makes the distinction clear.

by others, since that has already incurred an offloading cost $D_i(t)s_{ij}(t)c_{ij}(t)$. The amount of data collected by device i at time t and discarded is then $D_i(t)r_i(t)$, and the amount of data processed by each device i at time t is

$$G_i(t) = s_{ii}(t)D_i(t) + \sum_{j \neq i} s_{ji}(t-1)D_j(t-1).$$

In defining the variables $s_{ij}(t)$ and $r_i(t)$, we have implicitly specified the constraint $r_i(t) + \sum_j s_{ij}(t) = 1$: all data collected by device i at time t must either be processed by device i at this time, offloaded to another device j , or discarded. We assume that devices will not store data for future processing, which would add another cost component to the model.

2) *Data movement optimization*: We formulate the following cost minimization problem for determining the data movement variables $s_{ij}(t)$ and $r_i(t)$ over the time period T :

$$\begin{aligned} \text{minimize}_{s_{ij}(t), r_i(t)} \quad & \sum_{t=1}^T \left(\sum_i G_i(t)c_i(t) + \sum_{(i,j) \in E(t)} D_i(t)s_{ij}(t)c_{ij}(t) \right. \\ & \left. + \sum_i f_i(t)L(w_i(t)|D_V) \right) \end{aligned} \quad (5)$$

$$\text{subject to} \quad G_i(t) = s_{ii}(t)D_i(t) + \sum_{j \neq i} s_{ji}(t-1)D_j(t-1) \quad (6)$$

$$s_{ij}(t) = 0, \quad (i, j) \notin E(t), j \neq i \quad (7)$$

$$r_i(t) + \sum_j s_{ij}(t) = 1, \quad s_{ij}(t), r_i(t) \geq 0 \quad (8)$$

$$G_i(t) \leq C_i(t), \quad s_{ij}(t)D_i(t) \leq C_{ij}(t) \quad (9)$$

Constraints (6–8) were introduced above and ensure that the solution is feasible. The capacity constraints in (9) ensure that the amount of data transferred and processed are within link and node capacities, respectively. The three terms in the objective (5) correspond to the processing, offloading, and error costs, respectively, as we detail below.

(i) *Processing*, $G_i(t)c_i(t)$: This is the computing cost associated with processing $G_i(t)$ of data at node i at time t .

(ii) *Offloading*, $D_i(t)s_{ij}(t)c_{ij}(t)$: This is the communication cost incurred from node i offloading data to j .

(iii) *Error*, $f_i(t)L(w_i(t)|D_V)$: This cost quantifies the impact of the data movement on the error of the model at each device i ; note that since $w_i(t)$ is computed as in (3), it is an implicit function of $G_i(t)$, the data processed at device i . We include the error from *each* device i 's local model at each time t , instead of simply considering the error of the final model, since devices may need to make use of their local models as they are updated (e.g., if aggregations are infrequent due to resource constraints [5]). Discarding data clearly increases the loss, since less data is used to train the ML model; offloading may also skew the local model if it is updated over a small number of samples $G_i(t)$. We can, however, upper bound the loss function $L(w_i(t))$ regardless of the data movement:

Theorem 1 (Upper bound on the local loss). *If $L_i(w)$ is convex, ρ -Lipschitz, and β -smooth, if $\eta \leq \frac{1}{\beta}$, and if $L(w(T)) -$*

$L(w^) \geq \epsilon$ for some $\epsilon > 0$, then after K aggregations with a period τ and defining the constant $\delta_i \geq \|\nabla L_i(w) - \nabla L(w)\|$,*

$$L(w_i(t)) - L(w^*) \leq \epsilon_0 + \rho g_i(t - K\tau), \quad (10)$$

where $g_i(x) = \frac{\delta_i}{\beta}((\eta\beta + 1)^x - 1)$ implying $g_i(t - K\tau)$ is decreasing in K , and ϵ_0 is given by

$$\frac{1}{t\omega\eta(2 - \beta\eta)} + \sqrt{\frac{1}{t^2\omega^2\eta^2(2 - \beta\eta)^2} + \frac{Kh(\tau) + g_i(t - K\tau)}{t\omega\eta(1 - \beta\eta/2)}}.$$

Proof: Define $v_k(t)$ for $t \in \{(k-1)\tau, \dots, k\tau\}$ as the parameters under centralized gradient descent updates, $\theta_k(t) = L(v_k(t)) - L(w^*)$, $K = \lfloor t/\tau \rfloor$, and assume $\theta_k(k\tau) \geq \epsilon$ [5]. After lower-bounding $\frac{1}{\theta_{K+1}(t)} - \frac{1}{\theta_1(0)}$ and $\frac{1}{L(w_i(t)) - L(w^*)} - \frac{1}{\theta_{K+1}(t)}$, we can upper-bound $L(w_i(t)) - L(w^*)$ as

$$\left(t\omega\eta(1 - \frac{\beta\eta}{2}) - \frac{\rho}{\epsilon^2}(Kh(\tau) + g_i(t - K\tau)) \right)^{-1} = y(\epsilon).$$

Let ϵ_0 be the positive root of $y(\epsilon) = \epsilon$, which is easy to check exists. The result follows since either $\min_{k \leq K} L(v_k(k\tau)) - L(w^*) \leq \epsilon_0$ or $L(w_i(t)) - L(w^*) \leq \epsilon_0$; both imply (10).

For the full proof, see the supplementary materials. ■

In Section IV, we will consider how to use Theorem 1's result to find tractable forms of the loss expression that allow us to solve (5–9) efficiently and accurately. Indeed, without perfect information on the device costs, capacities, and error statistics over the time period T , it is not possible to solve (5–9) exactly. We will experimentally validate our proposed methods for estimating these network characteristics in Section V.

IV. OPTIMIZATION MODEL ANALYSIS

We turn now to a theoretical analysis of the data movement optimization problem (5–9). We discuss the choice of error and capacity values under various assumptions (Section IV-A), and then characterize the optimal solution for the ML use cases outlined in Section I (Section IV-B).

A. Choosing Costs and Capacities

We may not be able to reliably estimate the costs $c_{ij}(t)$, $c_i(t)$, and $f_i(t)$ or capacities $C_i(t)$ and $C_{ij}(t)$ in real time. Mis-estimations are likely in highly dynamic scenarios of mobile devices, since the costs $c_{ij}(t)$ of offloading data depend on network conditions at the current device locations. Mobile devices are also prone to occasional processing delays called “straggler effects” [19], which can be modeled as variations in their capacities. The error cost, on the other hand, will change over time as the model parameters move towards convergence. Here, we propose and analyze network characteristic selection methods. Although these methods also rely on some knowledge of the system, we show in Section V that a simple time-averaging of historical costs and capacities suffices to obtain reasonable data movement solutions.

1) *Choosing capacities*: Over-estimating the device processing capacities will force some data processing to be deferred until future time periods, which may cause a cascade of processing delays. Under- or over-estimations of the link capacities will have similar effects. Here, we formalize guidelines for choosing the capacities in (9)'s constraints so as to limit delays due to over-estimation. As commonly done [37], we assume that processing times on device stragglers follow an exponential distribution $\exp(\mu)$ for parameter μ .

For device capacities, we obtain the following result:

Theorem 2 (Data processing time with compute stragglers). *Suppose that the service time of processing a datapoint at node i follows $\exp(\mu_i)$, and that $c_{ij}(t)$, $c_i(t)$, $C_i(t)$ are time invariant. We can ensure the average waiting time of a datapoint to be processed is lower than a given threshold σ by setting the device capacity C_i such that $\phi(C_i) = \sigma\mu_i/(1 + \sigma\mu_i)$, where $\phi(C_i)$ is the smallest solution to the equation $\phi = \exp(-\mu_i(1 - \phi)/C_i)$, which is an increasing function of C_i .*

Proof: The processing at node i follows a D/M/1 queue with an arrival rate $G_i(t) \leq C_i$, and the result follows from the average waiting time in such a queue. The supplementary materials contains the full proof. ■

For instance, $\sigma = 1$ guarantees an average processing time of less than one time slot, as assumed in Section III's model. Thus, Theorem 2 shows that we can still (probabilistically) bound the data processing time when stragglers are present.

Network link congestion in transferring data may also delay its processing. Such delays can be handled by carefully choosing the network capacity analogously to Theorem 2's method.

2) *Choosing error expressions*: As shown in Theorem 1, we can bound the local loss at time t in terms of a gradient divergence constant $\delta_i \geq \|\nabla L_i(w) - \nabla L(w)\|$. The following in turn provides an upper bound for δ_i in terms of $G_i(t)$:

Lemma 1 (Error convergence). *Suppose that the distributions \mathcal{D}_i are non-iid so that $\mathcal{D}_i \neq \mathcal{D}_j$ for $i \neq j$, and that \mathcal{D} has finite second and third moments. Then there exists constants $\gamma_i > 0$ and $\gamma > 0$ that do not depend on the value of $G_i(t)$ and D_V respectively such that*

$$\delta_i \equiv \|\nabla L_i(w|G_i(t)) - \nabla L(w)\| \leq \frac{\gamma_i}{\sqrt{G_i(t)}} + \frac{\gamma}{\sqrt{|D_V|}} + \Delta \quad (11)$$

where $\Delta = \mathbb{E}(\mathcal{D}_i) - \mathbb{E}(\mathcal{D}_V)$ and $\gamma = \sum_{i=1}^N \gamma_i$

Proof: We first bound the local loss divergence by $\gamma_i/\sqrt{G_i(t)}$ and the global loss divergence by $\gamma/\sqrt{|D_V|}$, while Δ measures the difference between local and global distributions from which the samples are drawn.

If we now view each sample at device i as an i.i.d. sample of the data distributed at said device, then the result follows from the central limit theorem upon viewing each $\nabla l(w, x_d, y_d)$ as a sample from the distribution induced by $\nabla l(w|\mathcal{D}_i)$. ■

Combining the result in Lemma 1 with Theorem 1, we find that $L(w_i(t)) - L(w^*) \propto \sqrt{G_i(t)^{-1}}$. Thus, it is possible to take the error cost $f_i(t)L(w_i(t)|D_V)$ in (5) as $f_i(t)\sqrt{G_i(t)^{-1}}$

Use case	Topology	Dynamics
Smart factories [2]	Hierarchical	Fairly static
Connected vehicles [2]	Hierarchical	Rapid changes
Augmented reality [3]	Hierarchical, heterogeneous	Rapid changes possible
Privacy-sensitive [4], [19]	Social network	Fairly static

TABLE I: Dominant characteristics of the four use cases.

with $f_i(t)$ scaling the error importance; $f_i(t)$ may decrease over time as the model approaches convergence.

Since $\sqrt{G_i(t)^{-1}}$ is a convex function of $G_i(t)$, with this choice of error cost, (5–9) becomes a convex optimization problem and can be solved relatively easily in theory. When the number of variables is large, however – e.g., if the number of devices $n > 100$ with $T > 100$ time periods – standard interior point solvers will be prohibitively slow [38]. In such cases, we may wish to approximate the error term with a linear function and leverage faster linear optimization techniques, i.e., to take the error cost as $f_i(t)G_i(t)$ but with $f_i(t) < 0$ since the error decreases when $G_i(t)$ increases. If we neglect the offloaded data $s_{ij}(t)$ for $j \neq i$, we can rewrite this cost as $f_i(t)D_i(t)[1 - r_i(t)]$, which is equivalent to minimizing $-f_i(t)D_i(t)r_i(t)$. The error costs from the offloaded data can then be folded into the communication costs $c_{ij}(t)$, and we can approximate the error cost as $-f_i(t)D_i(t)r_i(t)$. Intuitively, discarding data implies a less accurate model.

B. Optimal Task Distributions

Given a set of costs and capacities for the optimization (5–9), we now characterize the optimal solutions in a range of practical cases. In particular, when we consider a linear error term $f_i(t)r_i(t)D_i(t)$, we have the following result:

Theorem 3 (Unconstrained resource solution). *Suppose that $C_i(t) \geq D_i(t) + \sum_{j \in \mathcal{N}_i(t-1)} D_j(t-1)$ for each device i , i.e., its compute capacity always exceeds the data it collects as well as any data offloaded to it by its neighbors $\mathcal{N}_i(t-1) = \{j : (j, i) \in E(t-1)\}$. Then if the error cost is linearly approximated as $f_i(t)D_i(t)r_i(t)$, the optimal $s_{ij}^*(t)$ and $r_i^*(t)$ will each be 0 or 1, with the conditions for 1 at node i being:*

$$\begin{cases} s_{ik}^*(t) = 1 & \text{if } c_{ik}(t) + c_k(t+1) \leq \min \{f_i(t), c_i(t)\} \\ s_{ii}^*(t) = 1 & \text{if } c_i(t) \leq \min \{f_i(t), c_{ik}(t) + c_k(t+1)\} \\ r_i^*(t) = 1 & \text{if } f_i(t) \leq \min \{c_i(t), c_{ik}(t) + c_k(t+1)\} \end{cases} \quad (12)$$

where $k = \arg \min_{j \neq i, (i,j) \in E(t)} \{c_{ij}(t) + c_j(t+1)\}$.

Proof: Since $r_i(t) + \sum_j s_{ij}(t) = 1$ in (8), each datapoint in $D_i(t)$ is either discarded, offloaded, or processed at i . It is optimal to choose the option with least marginal cost. ■

This theorem implies that in the absence of resource constraints, all data a device generates will either be processed, offloaded to the lowest cost neighbor, or discarded. Below, we examine implications of this result for typical fog topologies.

Fog use cases. Table I summarizes the topologies of the four fog applications from Section I. Networks in smart factories have fairly static topologies, since they are deployed in controlled indoor settings. They also exhibit a hierarchical

structure, with less powerful devices connected to more powerful ones in a tree-like manner, as shown in Figure 1. Connected vehicles have a similar hierarchical structure, with sensors and vehicles connected to more powerful edge servers, but their architectures are more dynamic as vehicles are moving. Similarly, AR applications feature (possibly heterogeneous) mobile AR headsets connected to powerful edge servers. Applications that involve privacy-sensitive data may have very different, non-hierarchical topologies as the links between devices are based on trust, i.e., comfort in sharing private information. Since social relationships generally change slowly compared to ML model training, these topologies are relatively static.

1) *Hierarchical topologies*: In hierarchical scenarios, more powerful edge servers will likely always have sufficient capacity $C_i(t)$ to handle all offloaded data (satisfying the assumptions in Theorem 3), and they will likely experience lower computing costs $c_i(t)$ as well compared to other devices. Theorem 3 indicates that, with a linear error cost, sensors would then offload their data to the edge servers, unless the cost of offloading the data exceeds the difference in computing costs. In Section V, we will see on our Raspberry Pi testbed that the network cost does indeed sometimes exceed the savings in computing cost from offloading to more powerful devices.

When the cost of discarding data is nonlinear, the optimal solution is less intuitive: it may be optimal to discard fractions of data if the reduction in error is not worth the additional cost of processing. Formally, in the case of a hierarchical topology, we have the following result:

Theorem 4 (Data movement with nonlinear error costs). *Suppose that n devices with identical, constant processing costs $c_j(t) = c$ and data generation rates $D_j(t) = D$ can offload their data to a single edge server, indexed as $n+1$. Further assume that there are no resource constraints, $c > c_{n+1}$, the costs $c_{ij}(t) = c_t$ of transmitting to the server are identical and constant, and the discard cost is given by $f_i(t)L(w_i(t)) = \gamma/\sqrt{G_i(t)}$ as in Lemma 1. Then, letting s denote the fraction of data offloaded, for D sufficiently large, the optimal amount of data discarded as a function of s is*

$$r^*(s) = 1 - \frac{1}{D} \left(\frac{\gamma}{2c} \right)^{\frac{2}{3}} - s. \quad (13)$$

Given the optimal r^* , the optimal s^* is given by

$$s^* = \frac{1}{nD} \left(\frac{\gamma}{2(c_{n+1} + c_t)} \right)^{\frac{2}{3}} \quad (14)$$

Proof: See supplementary materials for full proof. In the hierarchical scenario, the cost objective (5) can be rewritten as

$$n(1-r-s)Dc + nsD(c_{n+1} + c_t) + \frac{n\gamma}{\sqrt{(1-r-s)D}} + \frac{\gamma}{\sqrt{snD}}.$$

Taking the partial derivatives with respect to r and s , and noting that a large D forces $r, s \in [0, 1]$ gives the result. ■

Intuitively, as the costs c or c_{n+1} increase, so should the amount of data discarded. In the absence of computing costs, the processed data should be evenly distributed across the edge server and devices, so as to achieve similar errors at each



Fig. 3: Our Raspberry Pi devices running local computations.

device. This result contrasts with Theorem 3's, showing that more exact error bounds lead to a more even balance of data.

2) *Social network topologies*: When device networks are larger and have more complex topologies, we can extrapolate from Theorem 3's characterization of individual device behavior to understand data movement in the network as a whole. Consider, for instance, a social network of users in which edges are defined by willingness to share data (Figure 1b). We can find the probability that a given device offloads data, which allows us to determine the cost savings from offloading:

Theorem 5 (Value of offloading). *Suppose the fraction of devices with k neighbors equals $N(k)$, e.g., in a scale-free network $N(k) = \Gamma k^{1-\gamma}$ for some constant Γ and $\gamma \in (2, 3)$. Suppose $c_i \sim U(0, C)$ and $c_{ij} = 0$, where $U(a, b)$ is the uniform distribution between a and b , with no discarding. Then the average cost savings, compared to no offloading, equals*

$$\sum_{k=1}^n N(k) \left(\frac{C}{2} - \frac{C(-1)^k}{k+2} - \sum_{l=0}^{k-1} \binom{k}{l} \frac{C(-1)^l(k+3)}{(l+2)(l+3)} \right). \quad (15)$$

Proof: We first find $P_o(k)$ by computing the probability that at least one device j in the neighborhood of i has lower cost than c_i , from which we can determine (15). See the supplementary materials for details. ■

The processing cost model may for instance represent device battery levels drawn uniformly at random from 0 (full charge) to C (low charge). This result establishes that the reduction in cost from enabling device offloading in such scenarios is approximately linear in C : as the range of computing costs increases in a scale-free topology, there is greater benefit from offloading, since devices are more likely to find a neighbor with lower cost. The expected reduction, however, may be less than the average computing cost $C/2$ even in the absence of link costs, as offloading data to another device does not entirely eliminate the computing cost.

We finally consider the case in which resource constraints are present, e.g., for less powerful edge devices. We can find the expected number of devices with tight resource constraints:

Theorem 6 (Probability of resource constraint violation). *Let $N(k)$ be the number of devices with k neighbors, and for each device i with k neighbors, let $p_k(n)$ be the probability that its neighbor j has n neighbors. Also let \tilde{C} denote the distribution of resource capacities, assumed to be i.i.d. across devices, and let $D_i(t) = D$ be constant. Then if devices offload as in Theorem 3, the expected number of devices whose capacity*

Framework	Synthetic Costs		Real Costs	
	MLP (%)	CNN (%)	MLP (%)	CNN (%)
Centralized	92.00	98.00	92.00	98.00
Federated	89.67	96.45	89.67	96.45
Network-aware	88.63	95.89	89.70	96.03

TABLE II: Network-aware learning achieves comparable accuracy to both centralized and federated learning on test datasets.

constraints are violated is

$$\int_{\tilde{C}(x)} \left(\sum_{k=1}^N N(k) \mathbb{P} \left[1 - P_o(k) + k \sum_{n=1}^N \left(\frac{P_o(n)p_k(n)}{n} \right) \geq \frac{x}{D} \right] \right), \quad (16)$$

with $P_o(k)$ defined as the probability a device with k neighbors offloads its data.

Proof: This follows from Theorem 3 and determining the expected amount of data that will be processed at a node with k neighbors when offloading is enabled. ■

Theorem 6 allows us to quantify the complexity of solving the data movement optimization problem when resource constraints are in effect. We observe that it depends on not just the resource constraints, but also on the distribution of computing costs (through $P_o(k)$), since these costs influence the probability devices will want to offload in the first place.

V. EXPERIMENTAL EVALUATION

In this section, we experimentally evaluate our methodology in several scenarios. We discuss the experimental setup in Section V-A, investigate the baseline performance of network-aware learning in Section V-B, and examine the effects of network characteristics, structure, and dynamics in Sections V-C, V-D, and V-E respectively.

Aside from Table II, all other simulations rely exclusively on real data gathered from our testbed.

A. Experimental Setup

Data samples and ML models. We perform simulations using the MNIST dataset [39], which contains 70K images of handwritten digits. We use 60K of them as the training dataset D_V , and the remainder as our test set. The data generated at nodes $D_i(t)$ are modelled using a poisson arrival process with mean $\frac{|D_V|}{nT}$. Subsequently, each node is randomly allocated $|D_i(t)|$ datapoints from D_V , without replacement.

We train a multilayer perceptron (MLP) and a convolutional neural network (CNN) for image recognition on MNIST, with cross entropy loss [40] as the loss function $L(w|D_V)$, and constant learning rate $\eta(t) = 0.01$ as in (3). Unless otherwise stated, results are reported for CNN using an aggregation period $\tau = 10$ and $T = 100$ time intervals.

Costs and capacities. In the default case, we simulate $n = 10$ fog devices and one server. When imposed, the capacity constraints $C_i(t)$ and $C_{ij}(t)$ are defined as the average data generated per device, $\left\lfloor \frac{|D_V|}{nT} \right\rfloor$. Results are averaged over five iterations.

We consider both real and synthetic costs. Both real and synthetic error costs $f_i(t)$ are modelled using the accuracy

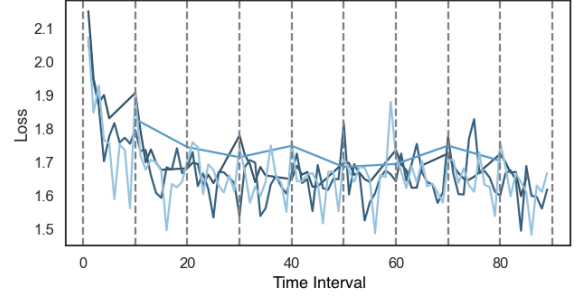


Fig. 4: Network-aware learning performance measured by loss recorded during training on real costs and capacities. The average and variance drop over time as expected.

Setting	Accuracy (%)	Cost				
		Process	Transfer	Discard	Total	Unit
A	89.72	1234	0	0	1234	0.265
B	89.81	322	120	167	609	0.125
C	89.54	302	117	160	580	0.126
D	83.14	336	63	268	667	0.136
E	82.83	307	46	282	635	0.137

TABLE III: Network costs and model accuracies obtained in four different settings. The differences between (A), where no data transfers are permitted, and (B)-(E), which are variants of network-aware learning, show substantial improvements in resource utilization.

measurements of historical runs done on the Raspberry Pi testbed. For the synthetic costs, $c_{ij}(t) \sim U(0, 1)$ and $c_i(t) \sim U(0, 1)$. The real-world measurements come from our testbed consisting of six Raspberry Pis using AWS DynamoDB as a cloud-based parameter server (Figure 3). Three Pis collect data and transmit it over bluetooth to another “gateway” Pi. The three gateway nodes receive this data and can either perform a local gradient update or upload the data to be processed in the cloud. We collect 100 sets of processing and communication measurements while training a two-layer fully connected neural network, with devices communicating over 2.4 GHz WiFi or LTE cellular. Gradient update processing time is linearly scaled to range from 0 to 1, comparable to the synthetic case, and then saved as $c_i(t)$. Raspberry Pi to DynamoDB communication time is similarly scaled then saved as $c_{ij}(t)$.

Centralized and federated learning. We compare network-aware learning against centralized learning, in which all data is processed at a single device (server), and standard federated learning, wherein data is fixed (i.e., $G_i(t) = D_i(t)$) and parameter aggregation occurs after every iteration ($\tau = 1$) [5], to determine if our method compromises learning accuracy by considering network costs as additional objectives. Results are discussed in Section V-B.

Perfect information vs. estimation. As discussed in Section IV-A, solving (5-9) in practice requires estimating the costs and capacities over the time horizon T . To do this, we divide T into L intervals T_1, \dots, T_L , and in each interval l , we use the time-averaged observations of $D_i(t)$, $p_i(t)$, $c_{ij}(t)$, and $C_i(t)$ over T_{l-1} to compute the optimal data movement. The resulting $s_{ij}^*(t)$ and $r_i^*(t)$ for $t \in T_l$ are then used by device i to transfer data in T_l . This “imperfect information” scheme will be compared with the ideal case of perfect information.

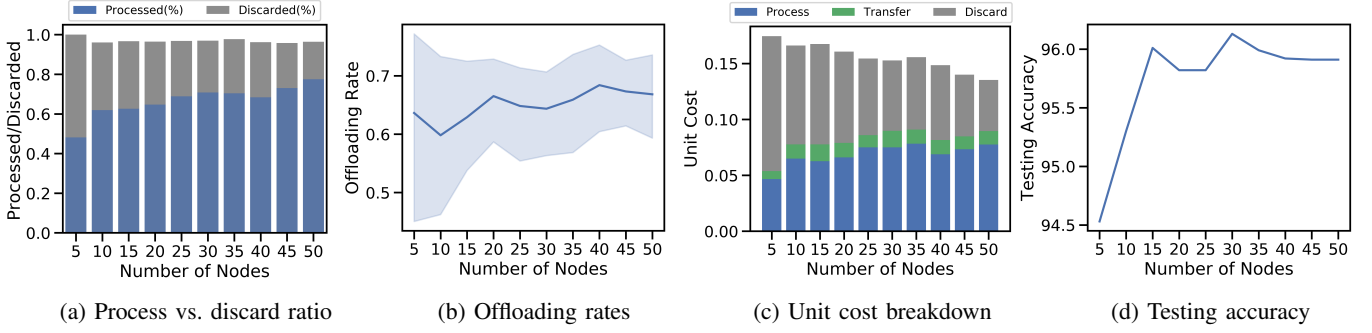


Fig. 5: Larger networks demonstrate increased data-efficiency, model accuracy and cost reduction. The shading in (b) shows the range over time periods. Network-aware learning scales well with the number of nodes, as the cost incurred per datapoint improves.

B. Efficacy of Network-Aware Learning

Our first experiments investigate the overall efficacy of our method. Here, we use the data-derived costs with a fully connected topology $E(t) = \{(i, j) : i \neq j\}$; similar results were observed with other configurations.

Model accuracy. Table II compares centralized, federated, and network-aware learning on both synthetic and real parameters. Additionally, the centralized and federated learning algorithms are run until convergence. The synthetic/real parameters comparison is included to provide a more thorough comparison between network-aware learning and state-of-the-arts, since network parameters only affect network-aware learning. Our method performs well: it achieves similar accuracy as federated learning and displays an inaccuracy of around 2% when compared against centralized learning.

The performance of network-aware learning at a local level is shown in Figure 4. The training loss $L_i(w_i(t))$ rapidly decreases over-time and, while some devices experience larger variance in their model loss, all devices exhibited an overall decreasing trend.

Network-aware learning produced more accurate models when using real rather than synthetic costs. Synthetic costs were more evenly distributed, i.e. nodes had neighbors with widely different costs, while real costs were linearized from actual processing and communication data, which preserves data extremes (e.g. devices with zero processing ability) and maintains the data’s inherent distribution. Our model will, therefore, likely perform better in real scenarios than in does in synthetic ones.

Offloading and imperfect information. Network-aware learning, even under imperfect information, can optimize network resources based on processing and communication costs to train ML models with reasonable accuracy when compared to federated learning. Table III compares the costs incurred and model accuracy for four settings: (A) offloading and discarding disabled, (B) network-aware learning with perfect information and no capacity constraints, (C) network-aware learning with imperfect information and no capacity constraints, (D) network-aware learning with perfect information and capacity constraints, and (E) network-aware learning with imperfect information and capacity constraints.

Costs in Table III are the aggregate costs over all nodes/links and time periods. The unit cost column is derived by dividing entries in the total cost column by that setting’s corresponding

total data. Simulations with imperfect information allocate data based on historical network characteristics, which may no longer be accurate, and can cause capacity excess issues. In capacity limiting cases, the excess data are discarded instead, incurring a corresponding discard cost. Yet this inefficiency only has a slight effect on the overall cost - see the 0.001 increase in unit cost from settings (D) to (E) and (B) to (C) in Table III.

Comparing (A) and (B), data transfers substantially reduces the unit cost— by 53%. The network took advantage of transfer links, reducing aggregate processing cost by 74%, by offloading more data. The accuracy in setting (B) marginally improves on (A) despite some datapoints being discarded: when offloading without capacity constraints, nodes with lower processing costs tend to receive significantly more data, giving them a larger sample size $G_i(t)$ for gradient updates, and thus more accurate parameter estimates that are also more heavily weighted in the aggregations. (D) and (E) re-introduce capacity constraints, resulting in both less accurate models and higher unit costs due to limited offloading capabilities. Strict capacity constraints limit the maximum transfers that can occur, leading to gradient updates based on fewer data. Finally, while there is a roughly 7% difference in accuracy between (A) and (E), note that the latter’s unit cost is only 51.7% of the former and that, if higher accuracy is desired, the error costs can be scaled to contribute more to minimizing the objective function.

C. Effect of Network System Characteristics

Our next experiments investigate the impact of n , the number of nodes, and the aggregation period, τ , on a fully-connected, fog topology. Then, we consider the effect of connectivity when nodes are connected in a random graph with probability ρ , i.e., $P[(i, j) \in E(t), j \neq i] = \rho$. For each experiment, we show (i) the fraction of data processed vs. discarded, (ii) the average fraction of data offloaded per node in each time interval, (iii) the unit costs, and (iv) the learning accuracy as we vary system characteristics.

Varying number of nodes n . The four subfigures in Figure 5 each show a specific characteristic of a fully-connected, resource-constrained network as it grows in size from five nodes to fifty nodes in increments of five nodes. Figure 5a depicts the growth in overall data processed; Figure 5b plots the change in the fraction of data that is offloaded to other

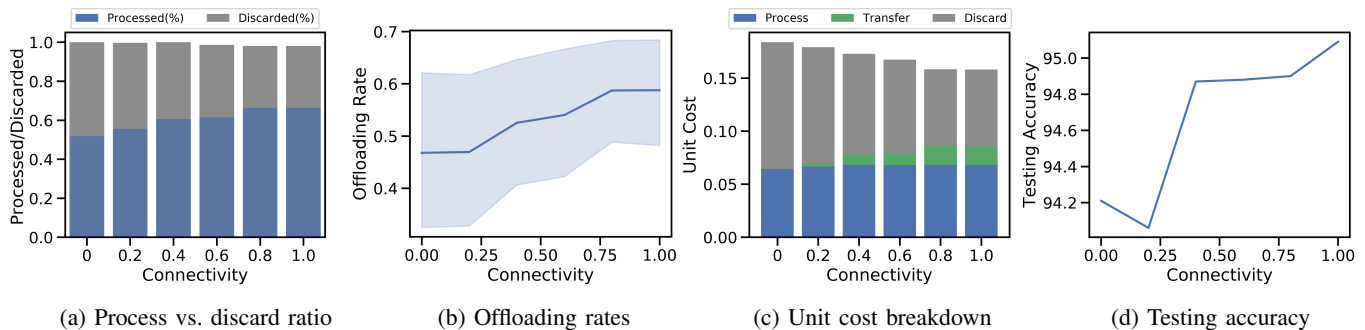


Fig. 6: Impact of the network connectivity ρ on data movement and costs in network-aware learning. Overall, we see that the costs are reasonably robust to ρ , with nodes offloading less frequently as ρ decreases. The learning accuracy, by contrast, tends to improve with ρ . The shading in (b) indicates the range over time periods.

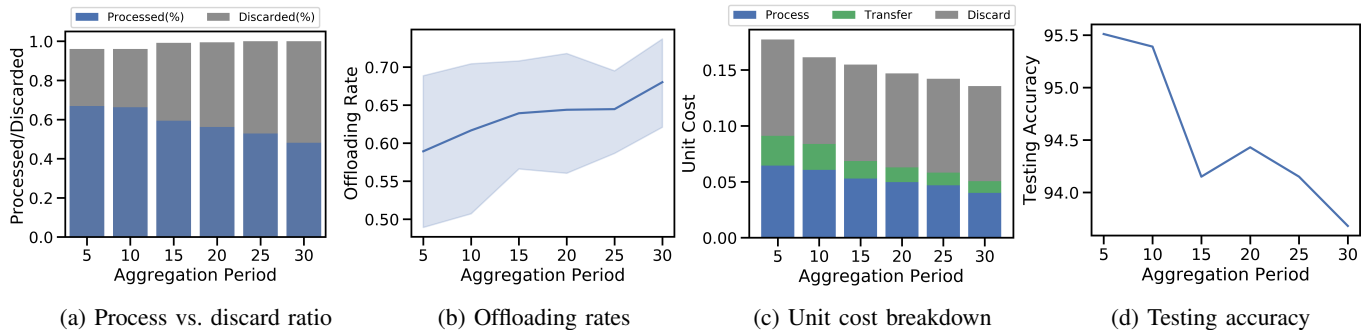


Fig. 7: Longer delays between aggregations τ result in decreased processing costs as local models converge, similar to Figure 3 in [5]. The shading in (b) indicates the range over time periods.

devices; Figure 5c provides a detailed breakdown of unit cost; and Figure 5d presents the resulting CNN model accuracy. The rounding used to address the optimization solver’s slight inconsistencies resulted in the variance in the sum of processed and discarded data ratios seen in Figure 5a.

As the network grows in size, the likelihood of connections between resource-constrained nodes to resource-abundant nodes increases, directly improving the quantity of cost-efficient data processing opportunities as per Theorems 5 and 6. Figure 5b highlights this trend as both the minimum offloading rate and the average offloading rate grows with network size. The unit cost per datapoint correspondingly decreases in Figure 5c. The processing cost now makes up a greater proportion of the total cost, because we are offloading data to be processed at more capable devices instead of discarding. Even though a larger fraction of data is being processed in Figure 5a, the increased processing cost incurred is outweighed by the savings in discard cost in Figure 5c. Finally, as a result of more data being processed, the training process produces a more accurate ML model in Figure 5d.

Varying network connectivity ρ . Figure 6 examines four characteristics of a resource-constrained network modelled as an Erdos-Renyi random graph with connectivity ρ varied from zero to one (i.e. from completely disconnected to fully-connected). As connectivity grows, Figures 6a and 6b see more data processed and a higher offloading rate, respectively. The unit cost per datapoint decreases in Figure 6c, caused by cheaper alternatives to discarding. Finally, Figure 6d shows a correlation between connectivity and testing accuracy.

Connectivity produces more opportunities for cost-efficient offloading in Figure 6a, which increases the total data pro-

cessed and decreases the total data discarded in Figure 6b. Discard costs also take a smaller share, relative to processing costs, of the unit costs in Figure 6c. Intuitively, more data processed leads to a more accurate model in Figure 6d. Increased network connectivity has a similar effect as having a larger network: there are more connections between resource-constrained nodes to resource-abundant nodes. Our scheme then takes advantage of these offloading opportunities to produce cost savings without compromising model accuracy.

Varying aggregation period τ . Figure 7 presents four characteristics of a fully-connected, resource-constrained network as the number of training iterations between aggregation cycles is increased from five iterations to thirty iterations in increments of five.

Local models converge as devices experience longer delays between aggregations, similar to the effects displayed in Figure 3 of [5]. Devices sample data from their local distributions for longer, eventually reaching convergence and reducing the value of processing each incremental datapoint. Since ML models at the devices converge, discarding becomes cost-effective in Figure 7a and the total discard cost takes a larger share of the unit cost in Figure 7c. Finally, because the total number of model iterations is kept static at $T = 100$, the longer aggregation periods result in a machine learning model with decreased accuracy in Figure 7d.

D. Effect of Fog Topology

Next, we evaluate network-aware learning on different fog computing topologies. We consider three different graph structures: hierarchical and social network topologies as in Section

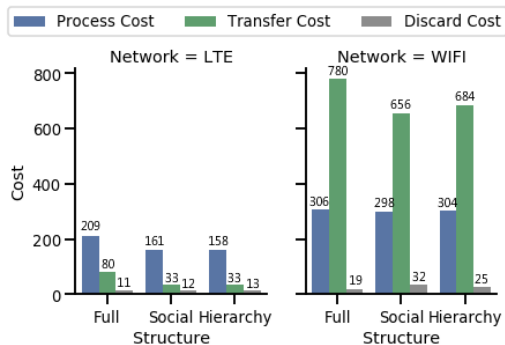


Fig. 8: Cost components for social, hierarchical, and fully connected topologies running network-aware learning on (a) LTE and (b) WiFi network media. Discard costs dominate for each topology in the case of WiFi, while those for LTE are more sensitive to topology.

IV-B, and, for completeness, a fully-connected topology in which all nodes are one hop neighbors of each other. The social network is modelled as a Watts-Strogatz small world graph [41] with each node connected to $n/5$ of its neighbors, and the hierarchical network connects each of the $n/3$ nodes with lowest processing costs to two of the $2n/3$ remaining nodes as leaves. We use the costs collected from our Raspberry Pi testbed, which provides two different wireless network media: LTE and WiFi.

The resulting costs are shown in Figure 8. Network topology determines the availability of cost-effective offloading opportunities. A fully-connected topology maximizes the degree of each node while a hierarchical topology minimizes the average degree (in our simulations). As the average degree becomes smaller, desirable offloading opportunities become scarcer, leading to decreases in transfer cost and increases in processing and discard cost as transferred data becomes locally processed or discarded instead.

Both LTE and WiFi exhibit similar behavior, however WiFi skews more heavily towards discarding. WiFi has fewer interference mitigation techniques than cellular, so, in the presence of several devices, we expect its links to exhibit longer delays. Consequently, both the discard and transfer costs are larger for WiFi than their LTE counterparts for fully-connected, social, and hierarchical network structures in 8. Results in both cases are consistent with the findings in Figure 6. As networks become less connected and edges grow sparse, the ability of individual devices to offload their data to lower cost alternatives diminishes. Devices will marginally increase their data processing workload but ultimately the majority of the data is discarded.

E. Effect of Dynamic Networks

Dynamic networks are assumed to have, at all time-steps, nodes entering or exiting uniformly at random with probabilities p_{entry} and p_{exit} . We assume that nodes cannot transmit their gradient descent results just prior to exiting the network and that nodes must wait for the ongoing aggregation period to finish when they initially join the network, in order to obtain up-to-date global parameters. Unless otherwise stated, all simulations in this section have $n = 10$ and $\tau = 10$ on a fully-connected topology.

Setting	Acc(%)	Nodes	Cost			
			Process	Transfer	Discard	Unit
Static	95.83	10	399	66	328	0.135
Dynamic	94.79	7.8	300	56	256	0.144

TABLE IV: Comparison of Network-Aware Learning Characteristics on Static and Dynamic Networks. “Acc” represents model accuracy and “Nodes” represents the average number of active nodes per aggregation period.

Table IV compares static versus dynamic networks with $p_{exit} = p_{entry} = 1\%$ as both networks train a CNN. Dynamic networks operate below optimal capacity, as the number of active nodes per aggregation period decreases from 10 in the static case to 7.8 in the dynamic case. Node exits always result in an inactive node - even if a new node enters, it must wait for the newest global parameters. Therefore, there is a loss of offloading opportunities and subsequent diminished overall processing power. More restrictive offloading leads to a 6% jump in effective costs incurred per datapoint. Although the total numerical costs decrease across all columns in Table IV, the fraction of costs due to discarding grows from 41.3% to 41.8% of total cost and those due to processing falls from 50.3% to 49% of total costs. Less processed data ultimately results in a model with poorer accuracy.

Next, Figure 9 eliminates the possibility of node entry to focus on the impacts of node exit and Figure 10 observes the effects of node entry by fixing node exit probability at 2%.

Varying probability of node exit p_{exit} . Results from five simulations with p_{exit} varied from 0% to 5% in increments of 1% and p_{entry} fixed at 0% were averaged to produce Figure 9. Aside from Figure 9a, the remaining four subfigures display similar information as those in Figures 5, 7, and 6.

Unstable networks are unlikely to maintain strong connections between nodes for an extended time. Figure 9a depicts a sharp decline in the number of active nodes per period as instability grows - the solid line is the average active nodes per period while the shaded area shows the range of active nodes per period. At 5% p_{exit} , the network has at most five active nodes/period.

Both total generated data and total cost decrease sharply with regards to exit probability in Figures 9b and 9d respectively. Since the network has fewer active nodes, there is less data overall and consequently total cost appear smaller. The ratio of processed versus discarded data indicates that more data is processed as the likelihood of node exit increases. A high exit probability slows convergence speed and, as per the analysis following Lemma 1, results in expensive discard costs. Due to both high discard costs and fewer opportunities for offloading, average offloading drops from 0.6 to 0.1 in Figure 9c. The resulting machine learning model declines in testing accuracy in Figure 9e as a result of less processed data. Inactive nodes bound the maximum amount of generated data and reduce offloading opportunities.

Varying probability of node entry p_{entry} . Probability of node entry is only relevant in dynamic networks with non-zero probability of node exit, hence, p_{exit} is fixed at 2% and p_{entry} is varied from 0% to 5%. Otherwise, the network is

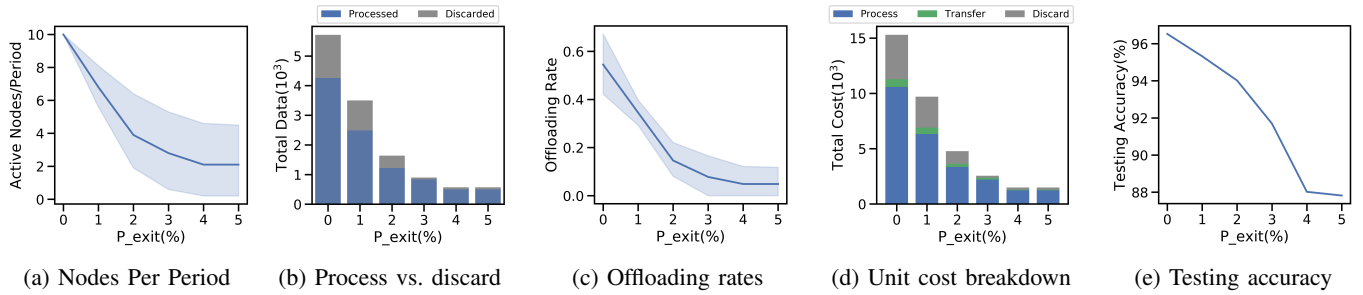


Fig. 9: Impact of increases in the probability of node exits on data movement and costs with $\tau = 10$ and probability of node entry of 0%. The shading in (a) and (c) indicates the range over time periods.

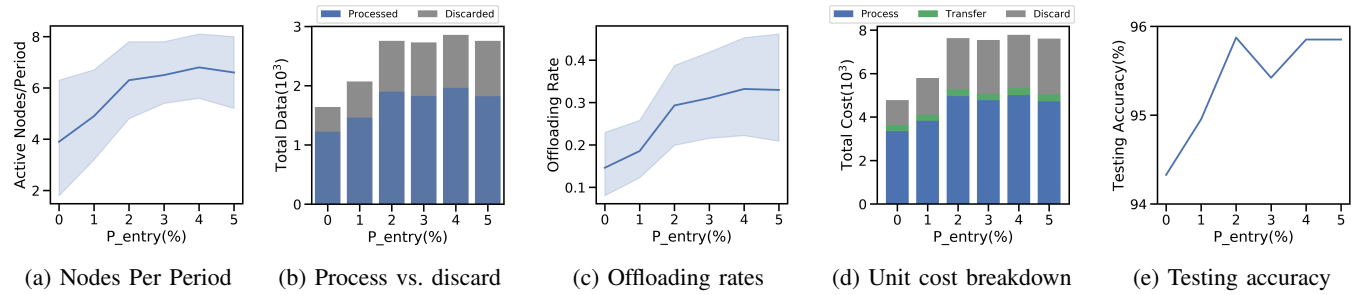


Fig. 10: Greater probability of node entry into networks results in increased model performance. The network has upper limit of ten nodes and $\tau = 10$ and probability of node exit of 2%. The shading in (a) and (c) indicates the range over time periods.

identical to that of Figure 9.

The average active nodes per period improves with probability of node entry until 2-3% in Figure 10a. Active nodes generate data and are possible offloading destinations. Consequently, there is growth in both total data generated in Figure 10b and average offloading rate in Figure 10c. The growth in total data directly results in higher total costs in Figure 10d. The availability of offloading opportunities allows data to be processed rather than discarded, ultimately helping the network produce a more accurate machine learning model in Figure 10e.

Comparing Figures 9 and 10, it seems that node exit impacts the network more heavily than node entry. For instance, in Figures 9a and 10a, node exit appears to influence active nodes/period more rapidly than node entry. Since we assumed worst-case behavior in a finite network, node entries experience an idle period and are effectively an inactive node until the next aggregation begins. Therefore, preventing exits is more important than promoting entry in “small” networks, such as our example with at most ten nodes. However, on size-unconstrained networks, a large p_{entry} may make more sense.

VI. CONCLUSION AND FUTURE WORK

To the best of our knowledge, this paper is the first work to distribute ML training tasks over devices in a fog computing network while considering the compute-communication trade-offs inherent in fog scenarios. We develop a framework to optimize the distribution of training tasks, taking into account both physical computing and communication costs and the error achieved by the models at each device. We derive new error bounds when devices can transfer their local data processing to each other, and theoretically bound the impact of these transfers on the cost and accuracy of the model training.

Through experimentation with a popular machine learning task, we show that our network-aware scheme significantly reduces the cost of model training while achieving comparable accuracy.

Our framework and analysis point to several possible extensions. First, while we do not observe significant heterogeneity in compute times on our wireless testbed, in general fog devices may experience compute straggling and failures, which might benefit from more sophisticated offloading mechanisms. Second, predicting devices’ mobility patterns and the resulting network connectivity can likely further optimize the data offloading. Finally, for some applications, one might wish to learn individual models for each device, which would introduce new performance tradeoffs between offloading and data processing.

ACKNOWLEDGMENT

This work was partially supported by NSF CNS-1909306 and the Army Research Office under grant W911NF1910036.

REFERENCES

- [1] Y. Tu, Y. Ruan, S. Wagle, C. Brinton, and C. Joe-Wong, “Network-Aware Optimization of Distributed Learning for Fog Computing,” in *IEEE Conference on Computer Communications (INFOCOM)*, 2020.
- [2] Cisco Systems, “Demystifying 5G in Industrial IOT,” White Paper, 2019. [Online]. Available: https://www.cisco.com/c/dam/en_us/solutions/iot/demystifying-5g-industrial-iot.pdf
- [3] D. Chatzopoulos, C. Bermejo, Z. Huang, and P. Hui, “Mobile Augmented Reality Survey: From where we are to where we go,” *IEEE Access*, vol. 5, pp. 6917–6950, 2017.
- [4] K. Rao, “The Path to 5G for Health Care,” *IEEE Perspectives on 5G Applications and Services*. [Online]. Available: <https://futurenetworks.ieee.org/images/files/pdf/applications/5G--Health-Care030518.pdf>
- [5] S. Wang, T. Tuor, T. Salonidis, K. K. Leung, C. Makaya, T. He, and K. Chan, “Adaptive Federated Learning in Resource Constrained Edge Computing Systems,” *IEEE Journal on Selected Areas in Communications*, vol. 37, no. 6, pp. 1205–1221, 2019.

- [6] M. Chiang and T. Zhang, "Fog and IoT: An Overview of Research Opportunities," *IEEE Internet of Things Journal*, vol. 3, no. 6, pp. 854–864, 2016.
- [7] IEEE Spectrum, "Applications of Device-to-Device Communication in 5G Networks," White Paper. [Online]. Available: <https://spectrum.ieee.org/computing/networks/applications-of-devicetodevice-communication-in-5g-networks>
- [8] M. Somisetty, "Big Data Analytics in 5G," IEEE Perspectives on 5G Applications and Services. [Online]. Available: <https://futurenetworks.ieee.org/images/files/pdf/applications/Data-Analytics-in-5G-Applications030518.pdf>
- [9] S. Pu, W. Shi, J. Xu, and A. Nedić, "A Push-Pull Gradient Method for Distributed Optimization in Networks," in *IEEE Conference on Decision and Control (CDC)*, 2018, pp. 3385–3390.
- [10] H. B. McMahan, E. Moore, D. Ramage, S. Hampson, and B. A. y Arcas, "Communication-Efficient Learning of Deep Networks from Decentralized Data," in *International Conference on Artificial Intelligence and Statistics (AISTATS)*, 2017.
- [11] T.-Y. Yang, C. Brinton, P. Mittal, M. Chiang, and A. Lan, "Learning Informative and Private Representations via Generative Adversarial Networks," in *IEEE International Conference on Big Data*. IEEE, 2018, pp. 1534–1543.
- [12] S. A. Ashraf, I. Aktas, E. Eriksson, K. W. Helmersson, and J. Ansari, "Ultra-Reliable and Low-Latency Communication for Wireless Factory Automation: From LTE to 5G," in *IEEE International Conference on Emerging Technologies and Factory Automation (ETFA)*, 2016, pp. 1–8.
- [13] S. Dutta, G. Joshi, S. Ghosh, P. Dube, and P. Nagpurkar, "Slow and Stale Gradients Can Win the Race: Error-Runtime Trade-offs in Distributed SGD," in *International Conference on Artificial Intelligence and Statistics (AISTATS)*, 2018, pp. 803–812.
- [14] J. Konečný, H. B. McMahan, F. X. Yu, P. Richtárik, A. T. Suresh, and D. Bacon, "Federated Learning: Strategies for Improving Communication Efficiency," in *Advances in Neural Information Processing Systems (NeurIPS)*, 2016.
- [15] R. Shokri and V. Shmatikov, "Privacy-Preserving Deep Learning," in *ACM Conference on Computer and Communications Security (SIGSAC)*, 2015, pp. 1310–1321.
- [16] P. Kairouz, H. B. McMahan, B. Avent, A. Bellet, M. Bennis, A. N. Bhagoji, K. Bonawitz, Z. Charles, G. Cormode, R. Cummings, R. G. L. D'Oliveira, S. E. Rouayheb, D. Evans, J. Gardner, Z. Garrett, A. Gascn, B. Ghazi, P. B. Gibbons, M. Gruteser, Z. Harchaoui, C. He, L. He, Z. Huo, B. Hutchinson, J. Hsu, M. Jaggi, T. Javidi, G. Joshi, M. Khodak, J. Konecny, A. Korolova, F. Koushanfar, S. Koyejo, T. Lepoint, Y. Liu, P. Mittal, M. Mohri, R. Nock, A. Zgr, R. Pagh, M. Raykova, H. Qi, D. Ramage, R. Raskar, D. Song, W. Song, S. U. Stich, Z. Sun, A. T. Suresh, F. Tramr, P. Vepakomma, J. Wang, L. Xiong, Z. Xu, Q. Yang, F. X. Yu, H. Yu, and S. Zhao, "Advances and open problems in federated learning," 2019.
- [17] Y. Zhao, M. Li, L. Lai, N. Suda, D. Civin, and V. Chandra, "Federated Learning with Non-IID Data," *arXiv:1806.00582*, 2018.
- [18] V. Smith, C.-K. Chiang, M. Sanjabi, and A. S. Talwalkar, "Federated Multi-Task Learning," in *Advances in Neural Information Processing Systems (NeurIPS)*, 2017, pp. 4424–4434.
- [19] G. Neglia, G. Calbi, D. Towsley, and G. Vardoyan, "The Role of Network Topology for Distributed Machine Learning," in *IEEE Conference on Computer Communications (INFOCOM)*, 2019, pp. 2350–2358.
- [20] J. Konecny, H. B. McMahan, F. X. Yu, P. Richtrik, A. T. Suresh, and D. Bacon, "Federated learning: Strategies for improving communication efficiency," 2016.
- [21] N. Strom, "Scalable distributed dnn training using commodity gpu cloud computing," in *Sixteenth Annual Conference of the International Speech Communication Association*, 2015.
- [22] A. F. Aji and K. Heafield, "Sparse communication for distributed gradient descent," *Proceedings of the 2017 Conference on Empirical Methods in Natural Language Processing*, 2017. [Online]. Available: <http://dx.doi.org/10.18653/v1/D17-1045>
- [23] F. Sattler, S. Wiedemann, K.-R. Müller, and W. Samek, "Robust and communication-efficient federated learning from non-iid data," 2019.
- [24] Y. Chen, X. Sun, and Y. Jin, "Communication-efficient federated deep learning with asynchronous model update and temporally weighted aggregation," 2019.
- [25] A. Lalitha, O. C. Kilinc, T. Javidi, and F. Koushanfar, "Peer-to-peer federated learning on graphs," 2019.
- [26] N. H. Tran, W. Bao, A. Zomaya, M. N. H. Nguyen, and C. S. Hong, "Federated Learning over Wireless Networks: Optimization Model Design and Analysis," in *IEEE Conference on Computer Communications (INFOCOM)*, 2019, pp. 1387–1395.
- [27] T. Chang, L. Zheng, M. Gorlatova, C. Gitaou, C.-Y. Huang, and M. Chiang, "Demo: Decomposing Data Analytics in Fog Networks," in *ACM Conference on Embedded Networked Sensor Systems (SenSys)*, 2017.
- [28] X. Ran, H. Chen, X. Zhu, Z. Liu, and J. Chen, "DeepDecision: A Mobile Deep Learning Framework for Edge Video Analytics," in *IEEE Conference on Computer Communications (INFOCOM)*, 2018, pp. 1421–1429.
- [29] C. Hu, W. Bao, D. Wang, and F. Liu, "Dynamic Adaptive DNN Surgery for Inference Acceleration on the Edge," in *IEEE Conference on Computer Communications (INFOCOM)*, 2019, pp. 1423–1431.
- [30] S. Teerapittayanon, B. McDanel, and H.-T. Kung, "Distributed Deep Neural Networks over the Cloud, the Edge and End Devices," in *IEEE International Conference on Distributed Computing Systems (ICDCS)*, 2017, pp. 328–339.
- [31] X. Xu, D. Li, Z. Dai, S. Li, and X. Chen, "A heuristic offloading method for deep learning edge services in 5g networks," *IEEE Access*, vol. 7, pp. 67 734–67 744, 2019.
- [32] H. Li, K. Ota, and M. Dong, "Learning iot in edge: Deep learning for the internet of things with edge computing," *IEEE Network*, vol. 32, pp. 96–101, 2018.
- [33] X. Wang, Y. Han, V. C. Leung, D. Niyato, X. Yan, and X. Chen, "Convergence of edge computing and deep learning: A comprehensive survey," *IEEE Communications Surveys & Tutorials*, 2020.
- [34] T. Yang, "Trading Computation for Communication: Distributed Stochastic Dual Coordinate Ascent," in *Advances in Neural Information Processing Systems (NeurIPS)*, 2013, pp. 629–637.
- [35] Y. Zhang, J. Duchi, M. I. Jordan, and M. J. Wainwright, "Information-theoretic Lower Bounds for Distributed Statistical Estimation with Communication Constraints," in *Advances in Neural Information Processing Systems (NeurIPS)*, 2013, pp. 2328–2336.
- [36] K. P. Murphy, *Machine Learning: A Probabilistic Perspective*. MIT Press, 2012.
- [37] F. Farhat, D. Z. Tootaghaj, Y. He, A. Sivasubramaniam, M. Kandemir, and C. R. Das, "Stochastic Modeling and Optimization of Stragglers," *IEEE Transactions on Cloud Computing*, vol. 6, no. 4, pp. 1164–1177, 2016.
- [38] F. M. F. Wong, Z. Liu, and M. Chiang, "On the Efficiency of Social Recommender Networks," *IEEE/ACM Transactions on Networking*, vol. 24, pp. 2512–2524, 2016.
- [39] Y. LeCun, C. Cortes, and C. J. C. Burges, "The MNIST Database of Handwritten Digits." [Online]. Available: <http://yann.lecun.com/exdb/mnist/>
- [40] Y. LeCun, B. Boser, J. S. Denker, D. Henderson, R. E. Howard, W. Hubbard, and L. D. Jackel, "Backpropagation Applied to Handwritten Zip Code Recognition," *Neural Computation*, vol. 1, no. 4, pp. 541–551, 1989.
- [41] M. Chiang, *Networked Life: 20 Questions and Answers*. Cambridge University Press, 2012.